ISSN 1674-1056
http://cpb.iphy.ac.cn
http://iopscience.iop.org/cpb
中国物理 B
Chinese Physics
中国物理
Chinese Physics B

Electronic properties of defects in Weyl semimetal tantalum arsenide

Yan-Long Fu(付艳龙), Chang-Kai Li(李长楷), Zhao-Jun Zhang(张昭军), Hai-Bo Sang(桑海波), Wei Cheng(程伟), Feng-Shou Zhang(张丰收)

Citation: Chin. Phys. B . 2018, 27(9): 097101. **doi:** 10.1088/1674-1056/27/9/097101

Journal homepage: http://cpb.iphy.ac.cn; http://iopscience.iop.org/cpb

What follows is a list of articles you may be interested in

Pressure effect in the Kondo semimetal $CeRu_4Sn_6$ with nontrivial topology

Jiahao Zhang(张佳浩), Shuai Zhang(张帅), Ziheng Chen(陈子珩), Meng Lv(吕孟), Hengcan Zhao(赵恒灿), Yi-feng Yang(杨义峰), Genfu Chen(陈根富), Peijie Sun(孙培杰)

Chin. Phys. B . 2018, 27(9): 097103. **doi:** 10.1088/1674-1056/27/9/097103

The effects of combining alloying elements on the elastic properties of *γ*-Ni in Ni-based superalloy: High-throughput first-principles calculations

Baokun Lu(路宝坤), Chongyu Wang(王崇愚)

Chin. Phys. B . 2018, 27(7): 077104. **doi:** 10.1088/1674-1056/27/7/077104

Magnetic interactions in a proposed diluted magnetic semiconductor $(Ba_{1-x}K_x)(Zn_{1-y}Mn_y)_2P_2$

Huan-Cheng Yang(杨焕成), Kai Liu(刘 凯), Zhong-Yi Lu(卢仲毅)

Chin. Phys. B . 2018, 27(6): 067103. **doi:** 10.1088/1674-1056/27/6/067103

First-principles investigations of proton generation in *α*-quartz

Yunliang Yue(乐云亮), Yu Song(宋宇), Xu Zuo(左旭)

Chin. Phys. B . 2018, 27(3): 037102. **doi:** 10.1088/1674-1056/27/3/037102

Uniaxial strain-modulated electronic structures of Cd*X* (*X*=S, Se, Te) from first-principles calculations: A comparison between bulk and nanowires

Linlin Xiang(相琳琳), Shenyuan Yang(杨身园)

Chin. Phys. B . 2017, 26(8): 087103. **doi:** 10.1088/1674-1056/26/8/087103

Electronic properties of defects in Weyl semimetal tantalum arsenide*

Yan-Long Fu(付艳龙)[1,2], Chang-Kai Li(李长楷)[1,2], Zhao-Jun Zhang(张昭军)[1,2], Hai-Bo Sang(桑海波)[1,2], Wei Cheng(程伟)[1,2,4,†], and Feng-Shou Zhang(张丰收)[1,2,3,‡]

[1] *Key Laboratory of Beam Technology of Ministry of Education, College of Nuclear Science and Technology, Beijing Normal University, Beijing* 100875, *China*
[2] *Beijing Radiation Center, Beijing* 100875, *China*
[3] *Center of Theoretical Nuclear Physics, National Laboratory of Heavy Ion Accelerator of Lanzhou, Lanzhou* 730000, *China*
[4] *Ningbo Institute of Industrial Technology, Chinese Academy of Sciences, Ningbo* 315201, *China*

(Received 23 March 2018; revised manuscript received 20 June 2018; published online 10 August 2018)

The tantalum arsenide (TaAs) is a topological Weyl semimetal which is a class of materials of gapless with three-dimensional topological structure. In order to develop a comprehensive description of the topological properties of the Weyl semimetal, we use the density functional theory to study several defects of TaAs after H irradiation and report the electronic dispersion curves and the density of states of these defects. We find that various defects have different influences on the topological properties. Interstitial H atom can shift the Fermi level. Both Ta vacancy with a concentration of 1/64 and As vacancy with a concentration of 1/64 destruct a part of the Weyl points. The substitutional H atom on a Ta site could repair only a part of the Weyl points, while H atom on an As site could repair all the Weyl points.

Keywords: Weyl semimetal, first-principles calculations, band structures, density of states

PACS: 71.15.Mb, 71.55.Ak, 73.20.At **DOI:** 10.1088/1674-1056/27/9/097101

1. Introduction

Weyl fermions are massless opposite chiral quasiparticles with spin 1/2,[1–3] and the material containing this particle is called Weyl semimetals (WSM). The characteristic of WSM with a gapless metal is topological invariant, which is different from the classification of topological phases of insulators. More significant characteristic is that the crossing points of the valence and conduction bands as Weyl point[4–6] are degenerate at the Fermi level.[7–9] Weyl nodes are associated with chiral and protect the gapless surface state on the bulk boundary of the sample.[10] Theory predicts the interesting physical properties of WSM, such as the negative magnetoresistance and the discontinuous Fermi arcs due to the chiral anomaly of Weyl nodes.[11–23] In Ref. [24], $Rn_2Ir_2O_7$, pyrochlore, with all-in or all-out magnetic structure,[25] possessing 24 pairs of Weyl points, was initiated associated with WSM in condensed-matter materials. The Weyl points appear when this system undergoes the magnetic ordering transition. $HgCr_2Se_4$,[26] a relatively simple system, exhibited a pair of double-Weyl points[10,27–30] when this system was in a ferromagnetic phase with the appearance of quadratic band crossing. Recent band structure calculations predict a new family of WSMs which includes TaAs, TaP, NbAs, and NbP, possessing 12 pairs of Weyl points[27,31] in the transition-metal monoarsenides or monophosphides.[12,27,29,32–35] In their lattice forms, these systems hold the time-reversal symmetry, while breaking the inversion symmetry. For all the properties mentioned above, of particular interest are the topological surface states of TaAs and isostructural crystal compounds TaP, NbP, and NbAs, which are experimentally investigated by the angle resolved photoelectron spectroscopy (ARPES)[29,36,37] pointing to the existence of the Weyl nodes.[27] Moreover, there is no magnetic effect caused by the complexity of the domain, or more directly, from their bulk electronic band structures by means of sensitive ARPES measurements.[36,38]

All of the above four materials have very similar band structures. First-principles calculations point to TaAs as a topological semimetal. In real materials, this is of great help to the exploration of Weyl physics. TaAs symbolizes a novel topological state of matter arousing interest in fundamental physics, and it has been verified to exhibit unique electronic properties and energy band structures as well as high carrier mobilities.[39] However, knowledge about its electronic properties of defects lags far from the perfect lattice.

As an effective material modification technique, ion beam implantation plays an important role in the study of defective crystals. The modified properties are from defects generated. It is practical interest to investigate the defective properties of these topological materials. When the exposure of this material to H irradiation, it is worthwhile mentioning that there are various kinds of defects in TaAs irradiated by H. In the present study, we particularly focus on these static point de-

*Project supported by the National Natural Science Foundation of China (Grant Nos. 11635003, 11025524, and 11161130520), the National Basic Research Program of China (Grant No. 2010CB832903), and the European Commissions of 7th Framework Programme (FP7-PEOPLE-2010-IRSES) (Grant No. 269131).

†Corresponding author. E-mail: chengwei@bnu.edu.cn
‡Corresponding author. E-mail: fszhang@bnu.edu.cn

© 2018 Chinese Physical Society and IOP Publishing Ltd

fective structures. Investigation shows that the possible point defects which can be produced are: interstitial (I_H), vacancies (V_{Ta} and V_{As}), the substitutional H atom on a Ta site (H_{Ta}) and on an As site (H_{As}). As we know, H_{Ta} and H_{As} may not exist in thermodynamic equilibrium, while they can appear in the ion implantation process. In the current work, the defect concentration is 1/64 in all defective lattices. The effect of defects on topological properties was studied by analysing the dispersion curves and density of states of different defects.

2. Optimisation algorithm and crystal structures

In the process of optimizing crystal structure, we use Perdew–Burke–Ernzerhof (PBE) to parameterize the exchange–correlation functional within a generalized gradient approximation.[41–45] In the present study, since spin–orbit coupling (SOC) may conceal the Weyl band-crossings in this system, we can not easily find out the Weyl band-crossings different from the other points, which is inconsistent with our discussion about the influence of defects on the topological properties. Taking the above situations into account, we neglect SOC in the calculation.

In the task of customized geometry optimization, we select the convergence tolerance energy to less than 5.0×10^{-6} eV, set the cut-off energy as 600 eV, and choose K-space mesh to less than 0.02 nm^{-1} in each direction. The calculations were carried out by using the software CASTEP for the first-principle calculations.[46] We have chosen the ultrasoft pseudopotential which facilitates faster calculation to meet the requirements. Since Weyl point is mainly correlated to valence electron, the description of core electron is implemented using pseudopotential.

The crystal texture of TaAs is a body-centered-tetragonal structure, and its space group is $I4_1md$ (No. 109) which lacks inversion symmetry and nonsymmorphic. The other super-cell of defects are $Pmm2$ (No. 25) symmetrical space group. The measured lattice constants in the experiment are $a = 3.4348$ Å, $b = 3.4348$ Å, and $c = 11.6410$ Å.[27,40] Wyckoff positions for Ta and As are (0, 0, 0) and (0, 0, 0.417), respectively. The primitive cell parameters are based on experimental parameters, and the cell parameters were optimized in order to obtain an energy minimized lattice structure. After cell optimisation, we obtain the lattice constants $a = b = 3.487932$ Å and $c = 11.72503$ Å. Due to the small variation of the cell parameters, the position of the atom is optimized more precisely. Optimising $u = 0.41535$ for the As site results in good agreement between our calculations and experiment. We set the constants for the perfect and defective $2 \times 2 \times 2$ super-cell as $a = b = 6.8696$ Å and $c = 23.282$ Å. The optimized lattice parameters are listed in Table 1. Prior to optimizing the atomic positions, it is worthwhile mentioning that the parameters a and b were found unequal. This is due to the presence of stress in the crystal.

Table 1. Lattice parameters of perfect and defective crystals.

	TaAs(Exp.)[27,40]	TaAs	$Ta_{32}As_{32}$(Exp.)[27,40]	$Ta_{32}As_{32}$	$HTa_{32}As_{32}$ I_H	$Ta_{31}As_{32}$ V_{Ta}	$Ta_{32}As_{31}$ V_{As}	$HTa_{31}As_{32}$ H_{Ta}	$HTa_{32}As_{31}$ H_{As}
a/Å	3.4348	3.487932	6.8696	6.976038	6.983937	6.972358	6.964457	6.977009	6.956079
b/Å	3.4348	3.487932	6.8696	6.976038	6.976269	6.973589	6.963483	6.958429	6.967218
c/Å	11.6410	11.725030	23.2820	23.448498	23.464922	23.412359	23.394487	23.447923	23.388076

Figure 1 presents our established super crystal structure with five defects. The perfect super crystal including 32 Ta and 32 As atoms. In the near middle of the box, one H atom stays in the gap and we get a defective crystal structure I_H.

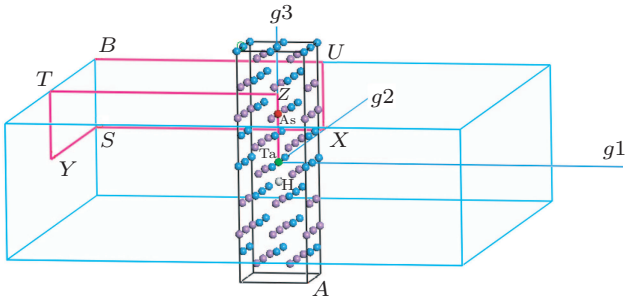


Fig. 1. (color online) Established super crystal structures of $Ta_{32}As_{32}$, I_H, V_{Ta}, V_{As}, H_{Ta}, and H_{As}. Inserting one gray H atom to the cell center results in defective structure I_H, removing one of the green Ta and red As atom results in the two defective structures V_{Ta} and V_{As} in near the center of the cell, and the substitutional H atom on a green Ta site and on a red As site results in the two defective structures H_{Ta} and H_{As} in near the center of the cell.

In the process of the H implantation, if one of the Ta and As atoms can be knocked out and H atom has enough energy to escape the lattice, we will obtain vacancy crystal structures V_{Ta} and V_{As}. In another case, if one of the Ta and As atoms can be knocked out and H atom just stays in Ta and As vacancy, we will get defective crystal structures H_{Ta} and H_{As}. In our calculation, all cell parameters and the atoms are free. In all the defective crystal structures, the lattice constants are almost identical and the symmetry is $Pmm2$ (No. 25).

3. Results and discussion

3.1. Defect formation energies

Before calculating the defect formation energy, we firstly optimize the energy for the five defects. Calculating the crystal energy of the optimized structure, we find that the energy differences for I_H, V_{Ta}, V_{As}, H_{Ta}, and H_{As} after and before optimization are −0.13 eV, −0.37 eV, −0.06 eV, −2.93 eV, and

−0.37 eV, respectively.

The defects have an effect on the electronic band structure, therefore various properties of the material may be affected. We calculate the crystal defect formation energy ΔH using the energy formula

$$\Delta H = E_{\text{def}} - E_{\text{bulk}} + \sum_i \Delta n_i \mu_i, \tag{1}$$

where E_{def} and E_{bulk} represent the energy of the defective structure and the bulk energy of the perfect structure, respectively. μ_i represents the energy of the ith inserting atom or vacancy atom, and Δn_i represents that the number of each defective super-cell is changed in the defect formation energy.[47,48]

Five defect formation energies are calculated similar to Refs. [47] and [49], summarized in Table 2. In Ref. [49], the formation energy of native defects as a function of the chemical potential of anion As was observed. Here, we calculate the defect formation energies of five typical defects formed by H irradiation. The defect formation energies, in descending order, are followed by V_{As}, I_H, V_{Ta}, H_{Ta}, and H_{As}.

Table 2. Defect formation energy of various defects.

Defect structures	Formation energy/eV[47,49]
I_H	−3.26
V_{Ta}	2.75
V_{As}	3.45
H_{Ta}	0.97
H_{As}	0.11

After the H ions have slowed down, the H ions can stop in a cage or stop in a vacancy center and the vacancies can be annihilated. That the formation energy of I_H is −3.26 eV means that the most stable defective structure is I_H. The minus sign of formation energy means that H atoms are possible to stay in one of the cages. According to Table 2, the formation energies of V_{As} and V_{Ta} are 3.45 eV and 2.75 eV, respectively. This means that V_{As} is more difficult to form than V_{Ta}. Compared with other defect formation energies, the formation energies of vacancies can be relatively large. Therefore, it is relatively difficult that vacancies are formed. On Ta site or As site, the substitutional H atom is energetically favorable. The tendency of H atoms is to annihilate produced vacancies. When H occupies the Ta vacancy, the formation energy is lower by 1.78 eV. When H occupies the As vacancy, the formation energy is lower by 3.34 eV. This result shows that H atoms are easier to annihilate As vacancies than to annihilate Ta vacancies.

3.2. Band structures

We compute how crystal defects influence the position of the Fermi level relative to the so-called Weyl points. As can be seen from Fig. 2(a), the band structure of $Ta_{32}As_{32}$ is along with the high-symmetry directions in Fig. 1, and as well, we find out that there are clear band inversion and multiple band crossing near the Fermi level along TY, UX, and ZT lines. These three lines have four equivalent lines respectively in the first Brillouin zone. Therefore, the band-crossing points along TY, UX, and ZT have four equivalent points. In the present study, five kinds of defects are discussed.

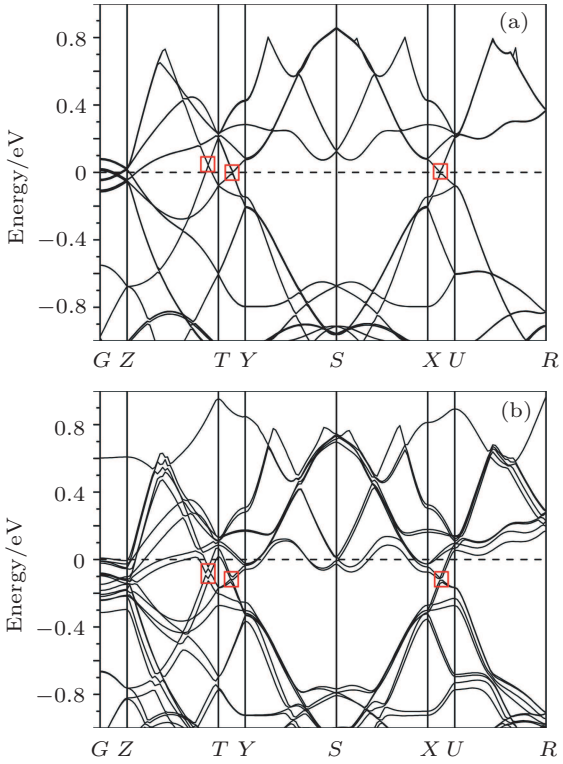


Fig. 2. (color online) Dispersion curves of (a) $Ta_{32}As_{32}$ and (b) $HTa_{32}As_{32}$. The Fermi level in panel (b) is almost 0.1 eV above that in panel (a). The square frames indicate the Weyl points.

3.2.1. I_H

I_H is represented by $HTa_{32}As_{32}$ with the symmetry group of $Pmm2$, in which H atom is an interstitial atom. The dispersion curve of a perfect super crystal is shown in Fig. 2(a) and the dispersion curve with a defect of H atom as an interstitial atom is shown in Fig. 2(b). As we can see from Fig. 2(b), the features of the band-crossings of Weyl points are fourfold degeneracy near the Fermi level along TY, UX, and ZT lines. However, the others are not located in corresponding area which are not Weyl points. Compared Fig. 2(b) with Fig. 2(a), it is found that the H atom can break the symmetry properties of TaAs and separate the degenerate curves. Although the bonding network of TaAs is stable, the electron interactions between surrounding host atoms and H atom are weak. To some extent, the degenerate bands become non-degenerate, which is linked to broken symmetry due to H atom. The band-crossing point along ZT line is sensitive to perturbation. The Fermi level was raised about 0.1 eV compared with pure TaAs. The reason for this is that H atom provides an extra electron which fills the bulk band of TaAs. In this case, the atomic concentration of a H atom is about 1/65. It is reasonable to

suppose that the Fermi energy can drop less when the concentration of H atoms decreases. As shown in Fig. 2(a), our calculated Weyl points that lie near the Fermi level are about $0.54/c$ at line TY and $0.46/c$ at line XU, respectively, which is consistent with experimental measurement.[50] The energies at G point extends to about 0.3 eV below the Fermi level, which is different from 0.2 eV for the perfect TaAs in Fig. 2(a). It is well known that one of the two degenerate bands will move up and the other will move down under perturbations, which suggests that the symmetry breaking interaction strength of interstitial is about 0.05 eV.

3.2.2. V_{Ta}

V_{Ta} is represented by $Ta_{31}As_{32}$ with the symmetry group of $Pmm2$, in which a Ta atom is removed from the center of the cell, and then a Ta vacancy cell is produced. The calculated dispersion curve of $Ta_{31}As_{32}$ is plotted in Fig. 3(a). Weyl points are located at about 0.3 eV above the Fermi level. The Fermi level is dropped because of the lack of Ta valence electrons. Compared vacancy with interstitial H, the shift of Fermi level is in opposite directions. It is shown that the band-crossings within lines TY and UX disappear. However, the band-crossing within line ZT still exists. When the concentration of Ta vacancy (1/64) is rather high, it is enough to destruct all the topological properties. The energies at G point extend to about 0.4 eV near the Fermi level, which is somewhat different from 0.2 eV for the perfect $Ta_{32}As_{32}$ in Fig. 2(a). This indicates that the interaction strength is symmetrically broken by about 0.1 eV for the Ta vacancy.

3.2.3. V_{As}

V_{As} is represented by $Ta_{32}As_{31}$ with the symmetry group of $Pmm2$, in which an As atom is removed from the center of the cell, and then an As vacancy cell is produced. The calculated dispersion curve of $Ta_{32}As_{31}$ is presented in Fig. 3(b). In this case, although the As vacancy almost does not affect the Fermi level, the observed asymmetry is significant. The band-crossings within lines ZT and TY still exist, while the band-crossing within line XU disappear. The As vacancy affects the topological properties less than Ta vacancy at the same vacancy concentration. The ground state electronic configurations of As and Ta are $[Ar]3d^{10}4s^24p^3$ and $[Xe]4f^{14}5d^36s^2$, respectively. Most known topological semimetals and topological insulators contain one heavy element at least. It is possible to conclude that the d and f electrons of Ta are the key to understanding the topological properties of TaAs. The energies at G point extend to about 0.3 eV near the Fermi level, which is different from 0.2 eV for the perfect $Ta_{32}As_{32}$ in Fig. 2(a). This indicates that the interaction strength is symmetrically broken by about 0.05 eV for the As vacancy. These phenomena suggest that the symmetry breaking interaction strengths of both vacancies is different in this material. Compared with Ta vacancy, the As vacancy has less impact on the topological properties.

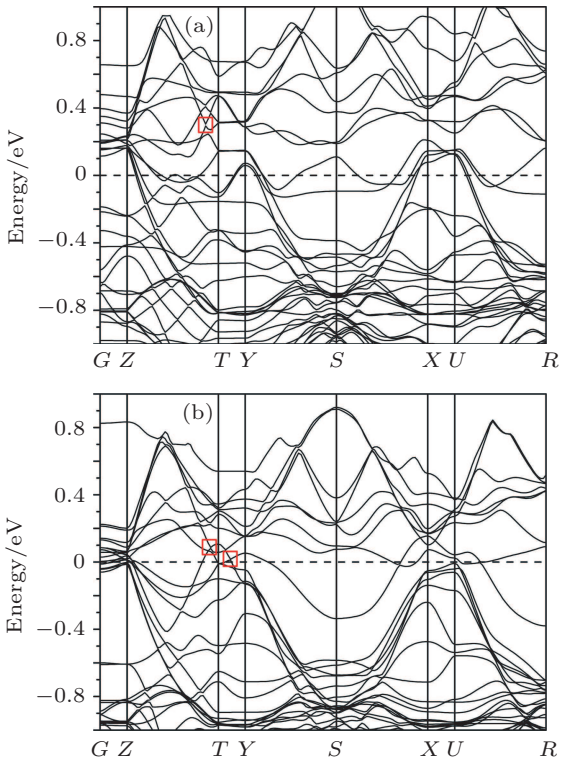


Fig. 3. (color online) Dispersion curves of (a) $Ta_{31}As_{32}$ and (b) $Ta_{32}As_{31}$. The band-crossings within lines TY and UX disappear in panel (a) and the band-crossings within line XU disappear in panel (b). The square frames indicate the Weyl points.

3.2.4. H_{Ta}

H_{Ta} is represented by $HTa_{31}As_{32}$ with the symmetry group of $Pmm2$, in which H atom substitutes a Ta atom on the corresponding site. The calculated dispersion curve of $HTa_{31}As_{32}$ was plotted in Fig. 4(a). As compared with Fig. 3(a), H atom can raise the Fermi level about 0.1 eV. The band-crossings at XU is repaired by H, while the band-crossing at TY is not repaired. This phenomenon is similar to the role of H in I_H. The bonding networks of $HTa_{31}As_{32}$ and $Ta_{32}As_{32}$ are almost the same, while the Fermi level is shifted by H and the band-crossing at TY is broken by defect. Although the emergence of Ta vacancy brings dangling bonds, H atom can heal these bonds. In this case, the topological electronic properties can also be partially healed by H atom, because H as a substitutional atom provides only s electrons. To remove d and f electrons from a Ta atom in the perfect $Ta_{32}As_{32}$ is similar to the defect H_{Ta}. It is shown that both the d and f electrons play an important role in topological properties.

3.2.5. H_{As}

H_{As} is represented by $HTa_{32}As_{31}$ with a substitutional H atom on an As site, which has the symmetry group of $Pmm2$.

The calculated dispersion curve of $HTa_{32}As_{31}$ is plotted in Fig. 4(b).

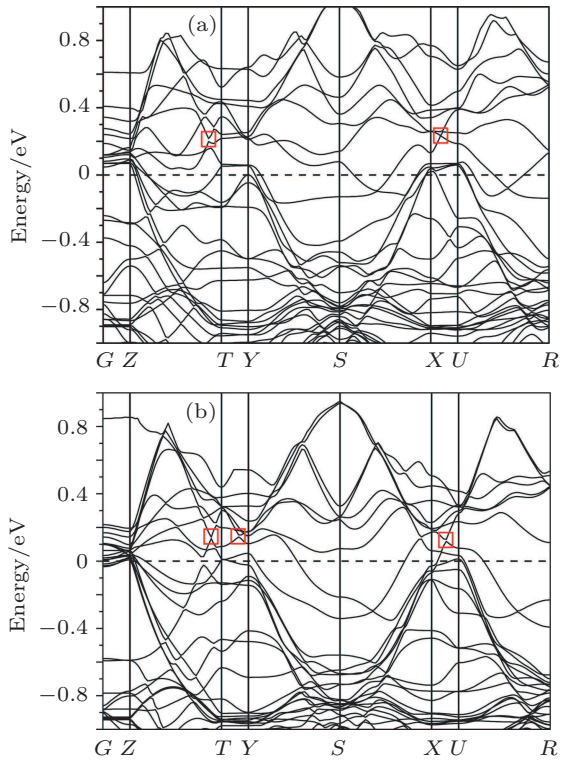


Fig. 4. (color online) Dispersion curves of (a) $HTa_{31}As_{32}$ and (b) $HTa_{32}As_{31}$. The band-crossings within line XU can be healed in panel (a). The band-crossing can be healed by H atom in panel (b). The square frames indicate the Weyl points.

In this case, all the Weyl points are identified, as seen in Fig. 4(b). As compared with Fig. 3(b), the band-crossings at TY, XU, and ZT all appear, and the Fermi level shifts down because H atom donates less electrons than As atom. The bonding network of $HTa_{32}As_{31}$ and $Ta_{32}As_{32}$ are almost the same, and the difference is that the Weyl points are located at about 0.1 eV above the Fermi level. Although further studies are required to clarify this question, a possible explanation is the fact that Weyl points approach the Fermi level when the concentration of substitutional H atom on an As site is lower than 1/64. The vacancy of As provides dangling bonds which H atom can heal. A credible explanation is that H atoms can heal the topological electronic properties. The recovery effect plays an extremely important role in the radiation resistant materials. To remove s and p electrons from an As atom in the perfect $Ta_{32}As_{32}$ is similar to the defect H_{As}. This suggests that the s and p electrons are less important for topological properties.

3.3. Density of states

As shown in Fig. 5, there are densities of states of different structures. We find that density of states for V_{As} is more close to TaAs than V_{Ta}. This indicates that the Ta atom is more important to the topological properties. At the same time, it must also be mentioned that H_{As} is close to V_{As} and H_{Ta} is close to V_{Ta}, and the differences of band dispersion both with and without H atom are small on near the Fermi level. It looks like that the interstitial H atom can only elevate the Fermi level of the bulk TaAs, and H atom with proper concentrations can fine-tune the Fermi level.

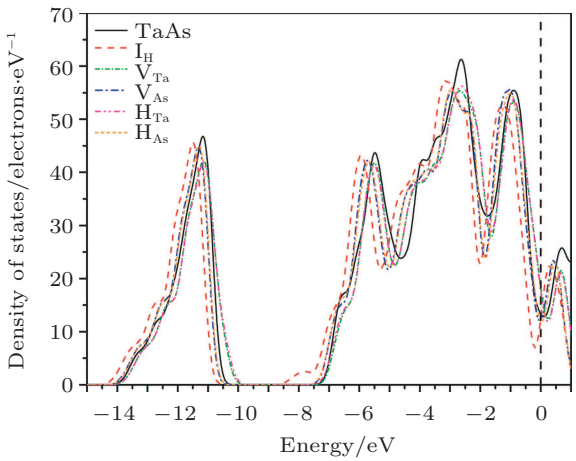


Fig. 5. (color online) Density of states of TaAs, I_H, V_{Ta}, V_{As}, H_{Ta}, and H_{As}.

The density of states curves of different orbits of the crystals are shown in Fig. 6. As compared with the partial density of states of the perfect crystal, the defective crystals have a higher density of states near the Fermi level. The density of states of s-orbit, p-orbit, and d-orbit are not zero on the Fermi level due to the lack of particle hole. Near the Fermi level, the smallest density of states of p-orbit and d-orbit of perfect TaAs are about 2 electrons/eV and 10 electrons/eV respectively, while the corresponding values of TaAs with defects are about 8 electrons/eV and 14 electrons/eV. The value of the density of states suggests that p and d electrons are more important than s electrons where topological properties are concerned. Our analysis shows the difference in the values of the smallest density of states of perfection and defects of 6 eV and 4 eV respectively, in terms of p and d electrons. This illustrates that several defects loss more p electrons than d and s electrons.

In addition, the specific focus is that the distribution of density of states near the Fermi level is destroyed by the defective atomic orbit hybridization.

4. Conclusion

The first principles calculations are performed to investigate its defect formation energies and explore the changes of topological properties, when H is injected into the perfect super-cell of TaAs. To the best of our knowledge, vacancies are more difficult to be formed than other defects. H is more efficient to repair the topological properties of As vacancies than Ta vacancies. The simulation results show that different

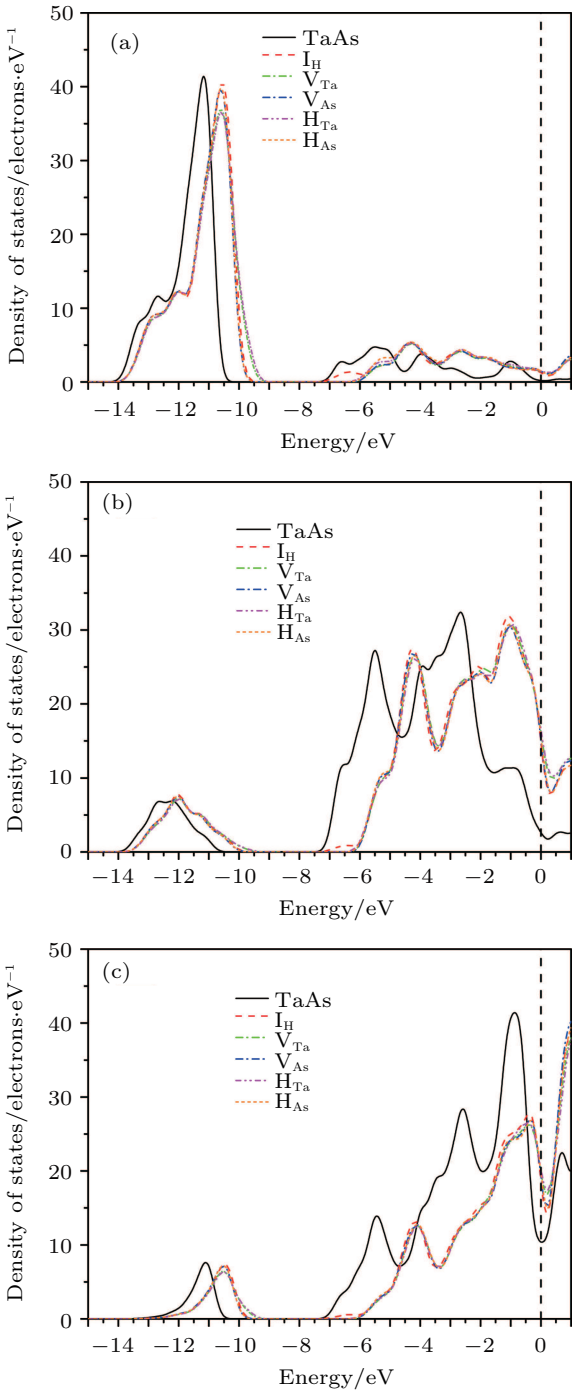


Fig. 6. (color online) Partial density of states of six super-cells of (a) s-orbit, (b) p-orbit, and (c) d-orbit.

defects have different influences on the topological properties. As H acts as an interstitial atom, it can shift the Fermi level. This phenomenon is interesting and further effort is required to understand the reason for shifted the Fermi level. Ta vacancy with a concentration of 1/64 or As vacancy with a concentration of 1/64 can destruct a part of the Weyl points. H atom on the Ta site can repair a part of the Weyl points, while the defect of substitutional H atom on an As site repairs all the Weyl points. The densities of states of $HTa_{32}As_{31}$ and $Ta_{32}As_{32}$ are almost the same near the Fermi level. A comparison of the curves of the density of states in different structures indicates that d and f electrons of Ta atom are most important to topological properties. The location of Weyl points is independent of types of defects. In addition, the Fermi level can be tuned by concentrations of vacancies and interstitial.

On the one hand, our results suggest that the Fermi level is regulated by changing the concentration of vacancy defects and interstitial atoms in TaAs, which may potentially be used to better separate electrons and holes in WSM. That the concentration of defects adjusts the Fermi level, therefore, provides a powerful method for topological material and is broadly applicable to a variety of systems. On the other hand, by thorough theoretical analysis, hydrogen can repair damaged Weyl points, which suggests its promising applications in reinforcing topological properties of materials and realizing electronic transmission with low energy consumption.

References

[1] Weyl H 1929 *Z. Phys.* **56** 330
[2] Xu B, Dai Y M, Zhao L X, Wang K, Yang R, Zhang W, Liu J Y, Xiao H, Chen G F, Taylor A J, Yarotski D A, Prasankumar R P and Qiu X G 2016 *Phys. Rev. B* **93** 121110
[3] Deb O and Sen D 2017 *Phys. Rev. B* **95** 144311
[4] Ahn S, Mele E J and Min H 2017 *Phys. Rev. B* **95** 161112
[5] Lu H Z and Shen S Q 2016 *Chin. Phys. B* **25** 117202
[6] He L P and Li S Y 2016 *Chin. Phys. B* **25** 117105
[7] Hasan M Z and Kane C L 2010 *Rev. Mod. Phys.* **82** 3045
[8] Fang C, Weng H M, Dai X and Fang Z 2016 *Chin. Phys. B* **25** 117106
[9] Hong G H, Wang C W, Jiang J, Chen C, Cui S T, Yang H F, Liang A J, Liu S, Lv Y Y, Zhou J, Chen Y B, Yao S H, Lu M H, Chen Y F, Wang M X, Yang L X, Liu Z K and Chen Y L 2018 *Chin. Phys. B* **27** 17105
[10] Hirayama M, Okugawa R, Ishibashi S, Murakami S and Miyake T 2015 *Phys. Rev. Lett.* **114** 206401
[11] Hosur P and Qi X 2013 *C.R. Phys.* **14** 857
[12] Lee C C, Xu S Y, Huang S M, Sanchez D S, Belopolski I, Chang G, Bian G, Alidoust N, Zheng H, Neupane M, Wang B, Bansil A, Hasan M Z and Lin H 2015 *Phys. Rev. B* **92** 235104
[13] Xu S Y, Belopolski I, Alidoust N, Neupane M, Bian G, Zhang C L, Sankar R, Chang G Q, Yuan Z J, Lee C C, Huang S M, Zheng H, Ma J, Sanchez D S, Wang B K, Bansil A, Chou F C, Shibayev P P, Lin H, Jia S and Hasan M Z 2015 *Science* **349** 613
[14] Igarashi A and Koshino M 2017 *Phys. Rev. B* **95** 195306
[15] Zyuzin A A and Zyuzin A Y 2017 *Phys. Rev. B* **95** 085127
[16] Shuichi M 2007 *New J. Phys.* **9** 356
[17] Singh B, Sharma A, Lin H, Hasan M Z, Prasad R and Bansil A 2012 *Phys. Rev. B* **86** 115208
[18] Liu J and Vanderbilt D 2014 *Phys. Rev. B* **90** 155316
[19] Kim H J, Kim K S, Wang J F, Sasaki M, Satoh N, Ohnishi A, Kitaura M, Yang M and Li L 2013 *Phys. Rev. Lett.* **111** 246603
[20] Zyuzin A A, Wu S and Burkov A A 2012 *Phys. Rev. B* **85** 165110
[21] Ojanen T 2013 *Phys. Rev. B* **87** 245112
[22] Son D T and Spivak B Z 2013 *Phys. Rev. B* **88** 104412
[23] Liang A J, Chen C Y, Wang Z J, Shi Y G, Feng Y, Yi H M, Xie Z J, He S L, He J F, Peng Y Y, Liu Y, Liu D, Hu C, Zhao L, Liu G D, Dong X L, Zhang J, Nakatake M, Iwasawa H, Shimada K, Arita M, Namatame H, Taniguchi M, Xu Z Y, Chen C T, Weng H M, Dai X, Fang Z and Zhou X J 2016 *Chin. Phys. B* **25** 77101
[24] Wan X, Turner A M, Vishwanath A and Savrasov S Y 2011 *Phys. Rev. B* **83** 205101
[25] Zhang H, Haule K and Vanderbilt D 2017 *Phys. Rev. Lett.* **118** 26404
[26] Xu G, Weng H, Wang Z, Dai X and Fang Z 2011 *Phys. Rev. Lett.* **107** 186806
[27] Weng H, Fang C, Fang Z, Bernevig B A and Dai X 2015 *Phys. Rev. X* **5** 011029
[28] Hosur P, Parameswaran S A and Vishwanath A 2012 *Phys. Rev. Lett.* **108** 046602
[29] Sun Y, Wu S C and Yan B 2015 *Phys. Rev. B* **92** 115428

[30] Liu Y, Prucnal S, Zhou S Q, Li Z L, Guo L W, Chen X L, Yuan Y, Liu F and Helm M 2016 *J. Magn. Magn. Mater.* **408** 73
[31] Huang S M, Xu S Y, Belopolski I, Lee C C, Chang G, Wang B, Alidoust N, Bian G, Neupane M, Zhang C, Jia S, Bansil A, Lin H and Hasan M Z 2015 *Nat. Commun.* **6** 7373
[32] Arnold F, Naumann M, Wu S C, Sun Y, Schmidt M, Borrmann H, Felser C, Yan B and Hassinger E 2016 *Phys. Rev. Lett.* **117** 146401
[33] Alidoust M, Halterman K and Zyuzin A A 2017 *Phys. Rev. B* **95** 155124
[34] Klotz J, Wu S C, Shekhar C, Sun Y, Schmidt M, Nicklas M, Baenitz M, Uhlarz M, Wosnitza J, Felser C and Yan B 2016 *Phys. Rev. B* **93** 121105
[35] Arnold F, Shekhar C, Wu S C, Sun Y, dos Reis R D, Kumar N, Naumann M, Ajeesh M O, Schmidt M, Grushin A G, Bardarson J H, Baenitz M, Sokolov D, Borrmann H, Nicklas M, Felser C, Hassinger E and Yan B 2016 *Nat. Commun.* **7** 11615
[36] Liu H W, Richard P, Song Z D, Zhao L X, Fang Z, Chen G F and Ding H 2015 *Phys. Rev. B* **92** 064302
[37] Lv B Q, Muff S, Qian T, Song Z D, Nie S M, Xu N, Richard P, Matt C E, Plumb N C, Zhao L X, Chen G F, Fang Z, Dai X, Dil J H, Mesot J, Shi M, Weng H M and Ding H 2015 *Phys. Rev. Lett.* **115** 217601
[38] Nakayama K, Kuno M, Yamauchi K, Souma S, Sugawara K, Oguchi T, Sato T and Takahashi T 2017 *Phys. Rev. B* **95** 125204
[39] Buckeridge J, Jevdokimovs D, Catlow C R A and Sokol A A 2016 *Phys. Rev. B* **93** 125205
[40] Xu S Y, Belopolski I, Sanchez D S, Neupane M, Chang G, Yaji K, Yuan Z, Zhang C, Kuroda K, Bian G, Guo C, Lu H, Chang T R, Alidoust N, Zheng H, Lee C C, Huang S M, Hsu C H, Jeng H T, Bansil A, Neupert T, Komori F, Kondo T, Shin S, Lin H, Jia S and Hasan M Z 2016 *Phys. Rev. Lett.* **116** 096801
[41] Perdew J P, Burke K and Ernzerhof M 1996 *Phys. Rev. Lett.* **77** 3865
[42] Wang Z, Sun Y, Chen X Q, Franchini C, Xu G, Weng H, Dai X and Fang Z 2012 *Phys. Rev. B* **85** 195320
[43] Sun Y, Zhang Y, Felser C and Yan B 2016 *Phys. Rev. Lett.* **117** 146403
[44] Lu M C, Guo Y N, Zhang M, Liu H Y and Tse J S 2016 *Solid State Commun.* **240** 37
[45] Gonze X 1995 *Phys. Rev. A* **52** 1096
[46] Clark S J, Segall M D, Pickard C J, Hasnip P J, Probert M J, Refson K and Payne M C 2005 *Z. Kristallogr.* **220** 567
[47] Yu Z G and Zhang Y W 2016 *Phys. Rev. B* **94** 195206
[48] Buckeridge J and Jevdokimovs D 2016 *Phys. Rev. B* **94** 180101
[49] Hong J H, Hu Z X, Probert M, Li K, Lv D H, Yang X N, Gu L, Mao N N, Feng Q L, Xie L M, Zhang J, Wu D Z, Zhang Z Y, Jin C H, Ji W, Zhang X X, Yuan J and Zhang Z 2015 *Nat. Commun.* **6** 18
[50] Lv B Q, Weng H M, Fu B B, Wang X P, Miao H, Ma J, Richard P, Huang X C, Zhao L X, Chen G F, Fang Z, Dai X, Qian T and Ding H 2015 *Phys. Rev. X* **5** 031013